# Uncovering the Roles of Oxygen in Cr(III) Photoredox Catalysis

Robert F. Higgins,[†] Steven M. Fatur,[‡] Samuel G. Shepard,[‡] Susan M. Stevenson,[§] David J. Boston,[†] Eric M. Ferreira,[§] Niels H. Damrauer,[‡] Anthony K. Rappé,*,[†] and Matthew P. Shores*,[†]

[†]Department of Chemistry, Colorado State University, Fort Collins, Colorado 80523-1872, United States
[‡]Department of Chemistry and Biochemistry, University of Colorado, Boulder, Colorado 80309-0215, United States
[§]Department of Chemistry, University of Georgia, Athens, Georgia 30602, United States

**S** *Supporting Information*

**ABSTRACT:** A combined experimental and theoretical investigation aims to elucidate the necessary roles of oxygen in photoredox catalysis of radical cation based Diels–Alder cycloadditions mediated by the first-row transition metal complex $[Cr(Ph_2phen)_3]^{3+}$, where $Ph_2phen$ = bathophenanthroline. We employ a diverse array of techniques, including catalysis screening, electrochemistry, time-resolved spectroscopy, and computational analyses of reaction thermodynamics. Our key finding is that oxygen acts as a renewable energy and



electron shuttle following photoexcitation of the Cr(III) catalyst. First, oxygen quenches the excited $Cr^{3+*}$ complex; this energy transfer process protects the catalyst from decomposition while preserving a synthetically useful 13 $\mu s$ excited state and produces singlet oxygen. Second, singlet oxygen returns the reduced catalyst to the Cr(III) ground state, forming superoxide. Third, the superoxide species reduces the Diels–Alder cycloadduct radical cation to the final product and reforms oxygen. We compare the results of these studies with those from cycloadditions mediated by related Ru(II)-containing complexes and find that the distinct reaction pathways are likely part of a unified mechanistic framework where the photophysical and photochemical properties of the catalyst species lead to oxygen-mediated photocatalysis for the Cr-containing complex but radical chain initiation for the Ru congener. These results provide insight into how oxygen can participate as a sustainable reagent in photocatalysis.
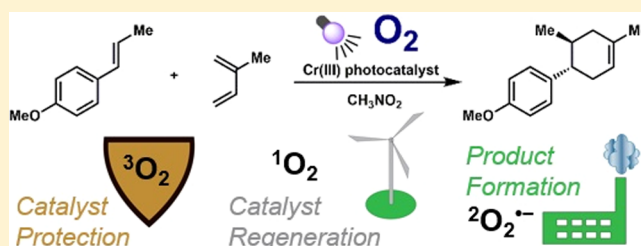
## INTRODUCTION

The resurgence of photoredox catalysis as a field of study reflects the importance of developing new or sustainable coupling reactions, where oxidative and reductive equivalents are selectively required within a mechanism but may not be introduced at the outset because of chemical incompatibility.[1−5] Most photoredox catalysts participate in one-electron processes and have been shown to promote a variety of transformations including cyclizations,[6,7] fluorinations,[8] and cross-couplings.[9,10] The most widely used catalysts contain Ru(II) and Ir(III) ions. However, there are limitations to the catalysts currently in use: The relative scarcity of Ir and Ru is often cited; in addition, catalysis employing those species can require stoichiometric excited-state trapping agents to increase the lifetime of the reducing or oxidizing agent.[11,12] Photosensitizers sourced from earth-abundant elements can also be challenged by short excited-state lifetimes.[13,14]

In situations where the exploitation of coreagents and/or promoters are required for photoredox catalysis, oxygen avails itself as an intriguing candidate because it is abundant and would simplify reaction setups; it would be ideal to perform reactions in air. Some reports propose oxygen as a replacement for commonly used oxidants such as ferric salts.[6,15] However, oxygen has several drawbacks: it often quenches excited states, it oxidizes metal-containing catalysts and/or photoinitiators, it leads to undesirable products via $O_2$ incorporation, and it is not

easy to monitor in reactions.[16−21] Some recent results invoke the importance of oxygen in photoredox catalysis. An exciting report by Yoon and co-workers used a Ru(II)-based system to promote a photoinduced Diels–Alder reaction using electron-rich dienophiles.[6] Oxygen was proposed as the sacrificial oxidant in the mechanism; however, the reaction proceeded without $O_2$, albeit in lower yield. Oxygen was also proposed as the terminal oxidant in a key step in the scaled-up synthesis of JAK2 Inhibitor LY2784544: oxygen concentration and/or mode of delivery had a significant impact on product yield as well as regioselectivity, but the precise role(s) of oxygen in the reaction pathway is an open question.[22] Another recent finding is the involvement of a trifluoroacetic acid-mediated oxygen oxidative quench of a Cu(I) excited state in the photocatalyzed $\alpha$-amino C–H bond functionalization.[23] Oxygen is proving to play an important role in photoredox chemistry, but the understanding of its function in these and related systems remains incomplete.

Multitool studies are contributing to our understanding of the nuances of reaction mechanisms in photoredox catalysis. Miranda and co-workers combined product studies, transient absorption spectroscopy, and electronic structure theory to probe an imino Diels–Alder reaction.[24] Very recently, Knowles

**Scheme 1. Initially Proposed Cycloaddition Pathways[a]**
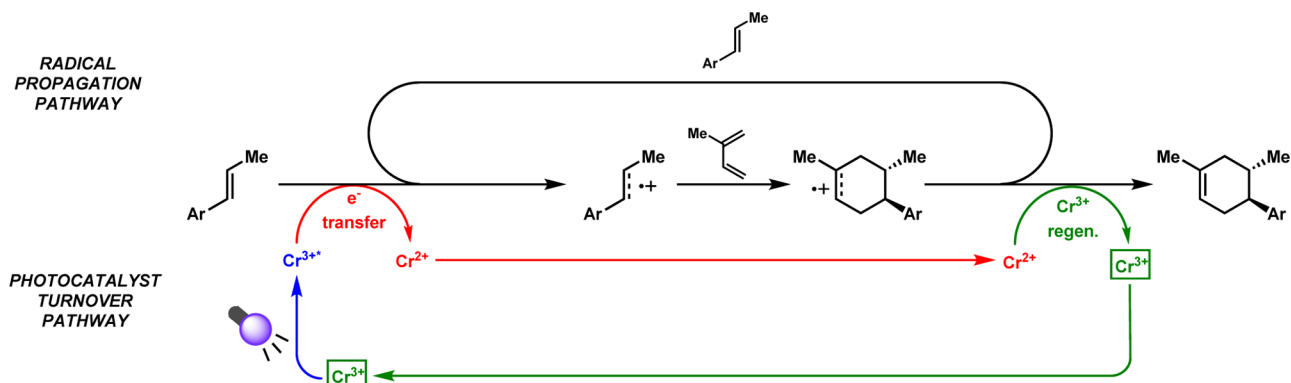


[a]The green boxes denote the initial form of the Cr-containing catalyst. Note that isoprene is shown in the form that appears in the cycloadduct; the *S*-trans form is the major species in solution.

**Scheme 2. Proposed Roles of Oxygen in Cycloaddition Pathways[a]**
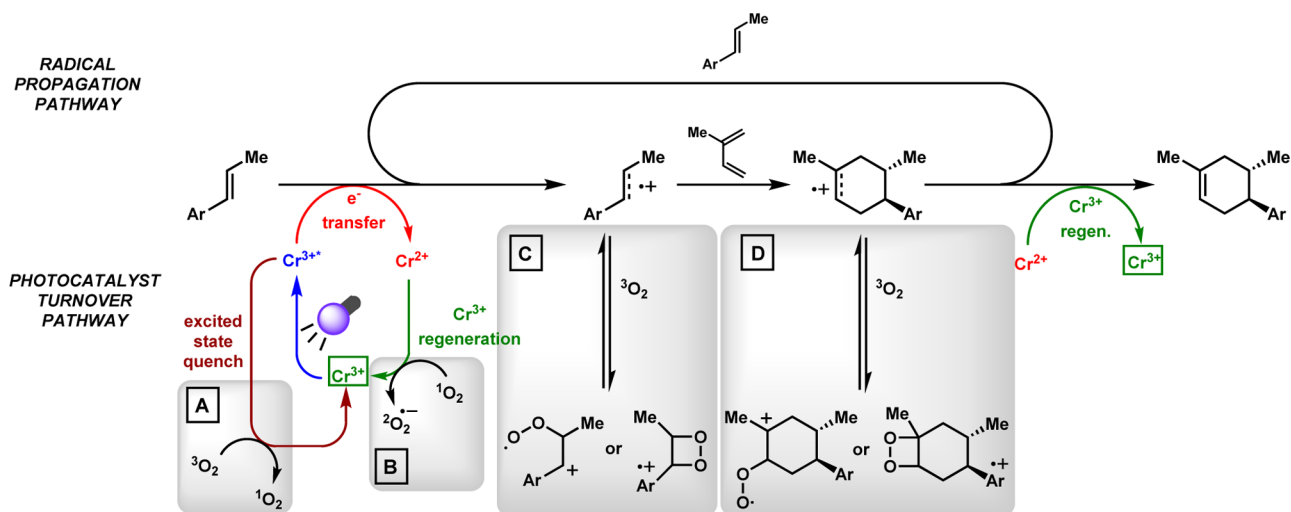


[a]The green boxes denote the initial form of the Cr-containing catalyst.

and co-workers reported an in-depth mechanistic study of the oxidation of an indoline to an indole promoted by an Ir(III) photocatalyst, enroute to the natural product Elbasvir.[25] Also, Peters and co-workers recently described the mechanism of a C−S cross-coupling reaction using a Cu photocatalyst.[26] Nevertheless, combined theoretical−experimental studies in this area remain uncommon.

Recently, some of us reported on a family of Cr(III) tris(aromatic diimine) complexes ([Cr]$^{3+}$) that could act as photocatalysts for Diels−Alder cycloadditions.[7] Taking advantage of the relatively long excited-state lifetimes found in these complexes (up to hundreds of microseconds),[27] we found that stoichiometric organic coreagents are not required to achieve catalysis. This combined with the employment of an earth-abundant metal ion provides a prototype for sustainable catalysis. In addition, we found that an intramolecular Diels−Alder reaction proceeded at good yield without byproducts, demonstrating that a chromium-based system offers differential reactivity with respect to Ru-based analogues.[6,7]

A preliminary attempt to describe the reaction pathway(s) as applied to the anethole−isoprene Diels−Alder cycloaddition is shown in Scheme 1. This mechanism implies an initial spin-allowed excitation of the Cr(III) complex [Cr]$^{3+}$ to a quartet

charge transfer excited state, followed by intersystem crossing to a long-lived doublet ($^2$E) excited state. The thus-prepared photoactive species [Cr]$^{3+*}$ could then oxidize the anethole (dienophile), while being reduced from [Cr]$^{3+}$ to [Cr]$^{2+}$.[28] The dienophile radical cation would couple with the diene to produce the cyclohexenyl radical cation. The product radical cation could either react with anethole to initiate a radical chain process or alternatively oxidize [Cr]$^{2+}$ to [Cr]$^{3+}$ to complete the catalytic cycle. In the radical chain process, the chain is terminated upon regeneration of the [Cr]$^{3+}$ species or reaction with another species in solution.

Importantly, this minimalist cycle does not account for our observation that molecular oxygen is required for photocatalytic turnover.[7] In principle, oxygen could oxidize the dienophile or diene to generate an organic radical cation, or perhaps it could oxidize the [Cr]$^{2+}$ complex, returning it to its resting state as [Cr]$^{3+}$. However, oxygen in aprotic media is not thermodynamically competent to oxidize any of these species: The O$_2$/O$_2^-$ couple in acetonitrile is −1.42 V vs Fc$^+$/Fc,[29,30] whereas the anethole$^{+/0}$, isoprene$^{+/0}$, and [Cr(Ph$_2$phen)$_3$]$^{3+/2+}$ couples occur at +1.0 V, +1.3 V, and −0.64 V vs Fc$^+$/Fc, respectively.[31−33] If singlet oxygen were somehow generated, then its excited state would add approximately +0.98 V of

oxidizing potential, which is still electrochemically insufficient to oxidize the organic substrates.

Notwithstanding, we can envision several thermodynamically feasible roles for oxygen in the catalytic cycle (Scheme 2), whether as quencher, redox shuttle, or stabilizer of intermediates.

Scenario **A** represents a potential source for singlet oxygen in the reaction mixture. Oxygen is well-documented to quench $^2[Cr]^{3+}$, forming $^1O_2$.[34] Excited state $^2[Cr]^{3+}$ is roughly 1.6 eV above ground-state $^4[Cr]^{3+}$ and $^1\Delta O_2$ is 0.98 eV more energetic than ground state $^3\Sigma O_2$,[35] consistent with facile energy transfer. In acetonitrile, $^1\Delta O_2$ has a relatively long lifetime of 40 $\mu s$.[36] For the proposed catalytic cycle, Cr excited-state quenching by $^3O_2$ may appear somewhat counterproductive, but the generation of $^1\Delta O_2$ could be important elsewhere. For example, scenario **B** makes use of $^1\Delta O_2$ as a potential route for catalyst regeneration. For $[Cr(Ph_2phen)_3]^{3+}$, the $[Cr]^{3+/2+}$ redox couple is −0.64 V vs $Fc^+/Fc$.[32] Thus, $^1\Delta O_2$ is competent to oxidize $[Cr]^{2+}$, whereas ground state $O_2$ is not. The combination of **A** and **B** represents a closed loop for singlet oxygen but should lead to a buildup of superoxide in the system, which could go on to reduce the product radical cation or another species in solution.

Alternatively or in addition, process **C** shows how molecular oxygen could stabilize the anethole radical cation, driving the oxidation reaction; such behavior has been suggested previously.[37] Relatedly, oxygen could stabilize the product radical cation (scenario **D**), and in turn could regenerate $[Cr]^{3+}$ or participate in a radical chain process. In both cases, superoxo species (left structures in **C** and **D**) and dioxetanes (right) represent possible intermediates.

Experiments addressing these and related options are presented and discussed below. We use a combination of synthesis screening, electrochemical and spectroscopic measurements, and finally electronic structure computations to determine oxygen's necessary role(s) in redox photocatalysis with a first-row transition-metal catalyst.

## ■ EXPERIMENTAL SECTION

**Preparation of Compounds.** Preparations of all metal complexes were performed inside a dinitrogen-filled glovebox (MBRAUN Labmaster 130). All catalysis screening reactions were performed in air. Acetonitrile (CH₃CN), tetrahydrofuran (THF), and dichloromethane (CH₂Cl₂) were sparged with dinitrogen, passed over alumina, and degassed before use. Nitromethane (CH₃NO₂) was sparged with dinitrogen and subjected to three freeze−pump cycles before use. Syringe filters were purchased from VWR international and were fitted with 0.2 $\mu m$ PTFE membranes. The compounds $[(CH_3CN)_4Cr-(BF_4)_2]$,[38] EtPPh₃Br,[7] (E)-1-methoxy-2-(prop-1-en-1-yl)benzene,[7] 4′-methoxy-2,4-dimethyl-1,2,3,6-tetrahydro-1,1′-biphenyl,[7] and 2′-methoxy-2,4-dimethyl-1,2,3,6-tetrahydro-1,1′-biphenyl[7] were synthesized according to literature preparations. Tetrabutylammonium hexafluorophosphate (Bu₄NPF₆) was recrystallized twice from ethanol before use. Ferrocene was sublimed before use. Anethole (**3**) is the trans isomer whenever used in this study. All other compounds and reagents were obtained commercially and were used as received.

**[Cr(Ph₂phen)₃](BF₄)₂ (1).** A solution of Ph₂Phen (250 mg, 0.752 mmol) in 8 mL of a 1:1 dichloromethane/acetonitrile mixture was added to $[(CH_3CN)_4Cr(BF_4)_2]$ (95 mg, 0.243 mmol) in 5 mL of acetonitrile. The solution color turned brown immediately. The reaction mixture was stirred for 1 h, and then it was filtered through a syringe. The filtrate was dried in vacuo. The crude product was recrystallized by diffusion of diethyl ether into a concentrated solution of acetonitrile to afford 232 mg (0.190 mmol, 78% yield) of brown crystals. UV−vis (CH₃CN) $\lambda_{max}$/nm ($\varepsilon_M$/M⁻¹ cm⁻¹): 428 (33 100),

490 (19 000), 572 (3060), 874 (16 600). IR (KBr pellet) $\nu_{C=N}$: 1618 cm⁻¹. ESI-MS(+) (CH₃CN): $m/z$ 1136.02 (M − BF₄)⁺. Anal. Calcd For $C_{72}H_{48}B_2F_8CrN_6$: C, 76.12; H, 4.26; N, 7.40. Found: C, 76.11; H, 4.09; N, 7.58.

**[Cr(Ph₂phen)₃](BF₄)₃ (2).** A solution of AgBF₄ (62 mg, 0.315 mmol) in 2 mL of acetonitrile was added to a solution of **1** (330 mg, 0.271 mmol) in 10 mL of acetonitrile. Over a period of 8 h, the color slowly changed from brown to orange and a gray precipitate (Ag metal) formed. The reaction mixture was filtered through Celite to remove the Ag metal, and the filtrate was concentrated in vacuo. Crystals were grown from a diethyl ether diffusion into a concentrated acetonitrile solution to yield 320 mg (0.245 mmol, 90% yield) of yellow crystals. UV−vis (CH₃NO₂) $\lambda_{max}$/nm ($\varepsilon_M$/M⁻¹ cm⁻¹): 378 (22700), 442 (2470), 488 (1320). IR (KBr pellet) $\nu_{C=N}$: 1624 cm⁻¹. ESI-MS(+) (CH₃CN): $m/z$ 1222.82 (M − BF₄)⁺. Anal. Calcd For $C_{72}H_{48}B_3F_{12}CrN_6$: C, 66.03; H, 3.69; N, 6.42. Found: C, 66.25; H, 3.46; N, 6.68.

**Electrochemical Measurements.** Electrochemical experiments were performed in 0.1 M solutions of Bu₄NPF₆ in CH₃CN, THF, CH₂Cl₂, and CH₃NO₂. Cyclic voltammograms (CVs) and square-wave voltammograms (SWVs) were recorded with a CH Instruments potentiostat (Model 1230A or 660C) using a 0.25 mm Pt disk or 0.25 mm glassy carbon disk working electrode, Ag⁺/Ag reference electrode, and a Pt wire auxiliary electrode. Scans were collected at rates between 10 mV/s and 2 V/s. Reported potentials are referenced to the $[Cp_2Fe]^+/[Cp_2Fe]$ (Fc⁺/Fc), where Cp = cyclopentadiene, redox couple, and were determined by adding ferrocene as an internal standard at the conclusion of each electrochemical experiment. Stirred solution experiments were performed using a disk stir bar positioned in close proximity to the working electrode. Oxygenated experiments were performed by bubbling O₂ into the experimentation vessel for 10 s prior to data collection. Dark experiments were performed by removing the vessel from all light for 20 min before and during scans. To help eliminate electrode interactions with possible superoxide species present, the working electrode was polished before each set of experiments were performed. The surface of the working electrode was also cleaned with a Kimwipe before each scan to help provide a clean surface of the electrode. Spectroelectrochemistry experiments were performed with an Ocean Optics DH-2000-BAL UV−vis−NIR spectrometer and a Gamry Instruments Reference 600 potentiostat via a Pine Instruments gold honeycomb electrode.

**Catalysis Studies.** In a representative cycloaddition experiment, a flame-dried 2 dram borosilicate vial open to air was charged with anethole (**3**, 17.7 mg, 0.120 mmol, 1 equiv), isoprene (**4**, 0.120 mL, 1.20 mmol, 10 equiv), [Cr(Ph₂phen)₃](BF₄)₃ (1.6 mg, 0.00120 mmol, 1 mol %), and nitromethane (1.20 mL, 0.10 M). The vial was capped and placed in a Rayonet photochemical reactor equipped with 419, 350, and 300 nm light bulbs. The reaction was irradiated with stirring until consumption of **3** was complete, as determined by TLC (27 h). The reaction was then diluted with H₂O (1.5 mL) and transferred to a separatory funnel. The layers were separated and the aqueous layer was extracted with Et₂O (3 × 2 mL). The combined organic layers were washed with brine (8 mL) and dried over Na₂SO₄. The volatile materials were removed by rotary evaporation, and the resulting residue was purified by flash chromatography (100% hexanes → 9:1 hexanes/EtOAc eluent) to afford cycloadduct 4′-methoxy-2,4-dimethyl-1,2,3,6-tetrahydro-1,1′-biphenyl (**5**, 22.7 mg, 88% yield) as a colorless oil. Performing the cycloaddition under more dilute conditions (0.033 M) resulted in a 59% yield of product **5** in 46 h.

**Mechanistic Measurements and Studies.** Reaction quantum yields and radical propagation chain lengths were determined by the method reported by Yoon and co-workers.[39] Actinometry experiments were performed using a Newport TLS-300XU tunable light source, which includes a 300 W Xe arc lamp, a Cornerstone 130 monochromator, and a motorized filter wheel; this instrument provides a wavelength range 250−2400 nm and wavelength selectivity of ±0.7 nm. Further experimental details are provided in the Supporting Information.

Emission lifetime measurements were conducted in nitromethane solutions of the catalyst at 0.1 absorbance and the indicated

concentration of quencher. The solutions were irradiated at 400 nm using the frequency doubled output from a 1 kHz repetition rate Ti:sapphire laser system, and emission was measured through a ~15 nm bandpass filter centered at 750 nm using a photomultiplier tube. The resulting decays were fit using a single exponential decay function. Air-free photochemical measurements were performed on samples prepared in a dinitrogen glovebox and placed in a 1 cm × 1 cm cuvette and sealed with a Teflon valve. Stern–Volmer methodology was employed to determine quenching rate constants from the experimental data. Details of these measurements are available in the Supporting Information.

Superoxide generation under $[Cr]^{3+}/[Cr]^{2+}/O_2$ photoirradiation conditions was probed by the method recently reported by Ivanović-Burmazović, Moënne-Loccoz, Goldberg, and co-workers.[40] A solution of **1** (12.72 mg) and **2** (4.55 mg, 3:1 mol %) in 2.5 mL of nitromethane was irradiated for 20 min (using a combination of 419, 350, and 300 nm sources) before an air outlet was administered, and 0.1 mL of thiophenol was added to the reaction mixture. After 30 min of stirring, the crude reaction mixture was filtered through a silica plug and concentrated in vacuo. The resulting filtrate was analyzed via $^1H$ NMR spectroscopy in $CDCl_3$, indicating ca. 88% yield of diphenyl disulfide. Exclusion of light, **1**, or oxygen resulted in minimal conversion of thiophenol to diphenyl disulfide (<5%). Details of these and related experiments are provided in the Supporting Information.

**Other Physical Measurements.** All experiments were conducted at room temperature unless otherwise noted. Absorption spectra were obtained with a Hewlett-Packard 8453 spectrometer in quartz cuvettes with a 1 cm path length. Infrared spectra were measured with a Nicolet 380 FT-IR spectrometer. Mass spectrometric measurements were performed in the positive ion mode on a Thermo LTQ mass spectrometer equipped with an analytical electrospray ion source and a quadrupole ion trap mass analyzer. Electron paramagnetic resonance (EPR) spectra were obtained using a continuous-wave X-band Bruker EMX 200U instrument outfitted with a liquid nitrogen cryostat. Compounds were dissolved in nitromethane and cooled to 120 K to acquire spectra. Elemental analyses were performed by Robertson Microlit Laboratories, Inc. in Madison, NJ.

**Electronic Structure Calculations.** The 6-311+g* basis set[41,42] and APFD hybrid density functional[43] were used to obtain the geometries, vibrational frequencies, and ideal gas thermodynamic estimates for the molecules computed. The APF hybrid density functional is an explicit linear combination of the B3PW91[44,45] and PBE0 (PBE1PBE)[46−48] hybrid functionals. The 41.1%:58.9% combination utilized was selected to minimize long-range artifacts present in standard functionals. The "D" spherical atom model dispersion term has been shown to reproduce large-scale CCSD(T) hydrocarbon intermolecular potential curves. The TD-DFT method[49] was used to obtain the excited state energies and oscillator strengths for $^3\mathbf{1}(BF_4)_2$, $^4\mathbf{2}(BF_4)_3$ **3**, $^2\mathbf{3}\cdot BF_4$, **5**, and $^2\mathbf{5}\cdot BF_4$. Natural transition orbitals (NTOs) were used to assess the character of the electronic transitions. The "from" and "to" NTOs were obtained through diagonalization of the transition density matrix transformed over the occupied and virtual spaces, respectively.[50] Reactions and structures involving isoprene were computed using the S-trans form of the molecule, which is the majority species in solution and chemically reactive. Reaction energetics of ionic species were computed including a charge-compensating ion, either $BF_4^-$ or $N(CH_3)_4^+$ (TMA). Further details are provided in the Supporting Information.

## ■ RESULTS

**Catalyst Syntheses.** As a representative example, we have focused our mechanistic studies on $[(Cr(Ph_2phen)_3]^{3+}$ because its photoredox properties are most comparable to those of Ir- and Ru-containing species and it promotes the highest cyclization yields in the initial report.[7] The divalent complex, $[Cr(Ph_2phen)_3](BF_4)_2$ (**1**), is prepared in a straightforward manner by combining stoichiometric quantities of

$[(CH_3CN)_4Cr(BF_4)_2]$ and $Ph_2phen$ in acetonitrile. Compound **1** is air-sensitive in solution: the color changes from brown to light yellow over 12 h when exposed to air, and bubbling $O_2$ into the solution initiates the color change within 30 s. Controlled oxidation of **1** with $AgBF_4$ under inert atmosphere successfully produces trivalent complex salt **2**. This represents the first one-pot method to produce a homoleptic chromium phenanthroline complex without caustic reagents, with a simpler procedure compared to literature reports.[32,51]

The absorption characteristics of **1** are quite different from complex **2**, as evidenced in Figure 1. Both complexes feature
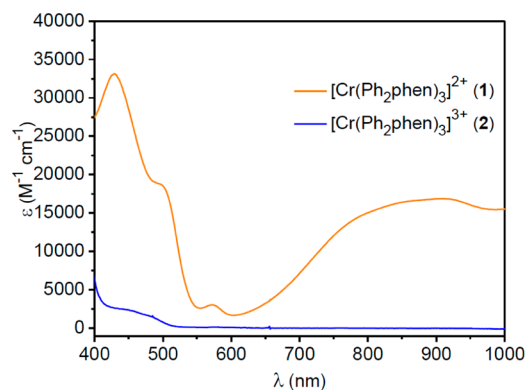


**Figure 1.** Electronic absorption spectra of **1** and **2** in $CH_3NO_2$.

$Cr^{3+}$ ions: the stronger absorption overall and the near IR bands found in **1** are consistent with one of the $Ph_2phen$ ligands acting as a radical anion in **1**, whereas all ligands are neutral in **2**.[32] Computed electronic spectra for **1** and **2** (Figures S51 and S52) as well as net spin density plots are provided in Figures S55 and S56. Meanwhile, other salts of **2** that have been prepared previously (OTf⁻ and Cl⁻) have nearly identical absorption spectra (Figure 1), indicating similar solution environments for the trivalent species irrespective of cation−anion interactions.

**Catalysis Studies.** As a representative reaction, the combination of **3** with **4** in nitromethane in the presence of catalytic amounts of **2**, light, and oxygen affords the cycloadduct **5** in 88% yield (Scheme 3). Conveniently, this reaction can be

**Scheme 3**
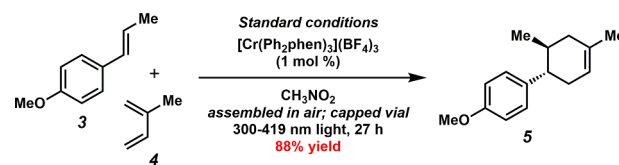
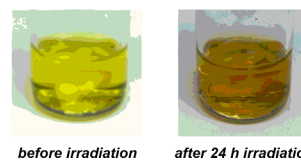

| Modification to standard conditions | Results[a] |
|---|---|
| no air[b] | 4% yield |
| no air[b], 20 mol % cat. | 8% yield |
| 10 mol % DMSO | 64% yield |
| 10 mol % benzoquinone | 34% yield[c] |

[a] $^1H$ NMR yields with dodecyl acetate as int. std.
[b] degassed by 3 freeze-pump-thaw cycles
[c] 27% trans-anethole remaining

*before irradiation*    *after 24 h irradiation*

set up open to air and then just capped. When the reaction is performed in the absence of air (reaction mixture degassed by three freeze−pump−thaw cycles prior to irradiation), only trace product is formed. Without an air inlet, the color of the reaction mixture changes from a bright yellow to a darker tannish color over time (Scheme 3). No product formation occurs when the reaction is performed without light. Furthermore, the addition of dimethyl sulfoxide or benzoquinone (the latter is a superoxide scavenger) significantly slows the reaction, and addition of 25 mol % benzoquinone results in only a 2% yield of product. As noted previously, the cyclization reaction proceeds in acetonitrile with slightly lower yield (70%). For comparison to the $[Ru(bpz)_3]^{2+}$-photoinitiated system,[6] performing the reaction in dichloromethane affords a comparable but lower yield after 27 h of irradiation (50%, Table S1). We also find that cycloadduct 5 can be formed in dimethylformamide (DMF). However, this solvent choice relates to spectroscopic studies (vide infra), and yields were not obtained.

Cycloadditions using terminally unsubstituted dienes proceed efficiently. In contrast, when terminally substituted dienes 8 and 10 are used, the additions occur much more efficiently when the reaction is performed with a needle air outlet compared to a sealed vial (Scheme 4). This observation indicates an important influence of air ($O_2$) depending on the nature of the reactants, namely, if cycloaddition is slowed.

**Scheme 4**
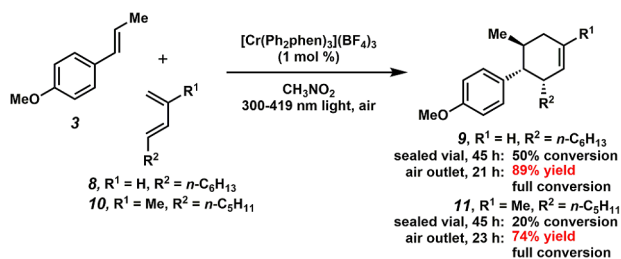


**Electrochemical Studies.** Cyclic voltammograms of 1 and 2 in catalytically relevant solvents are shown in Figure 2, and the electrochemical data are compiled in Table 1. All of the redox events observed appear to be single-electron processes. These assignments are supported by the peak-to-peak potential differences and similarity of currents passed in square wave voltammetry experiments (Figures S1, S6, and S11) and are consistent with literature precedent.[32]

The CV of divalent 1 in $CH_3NO_2$ (Figure 2, red trace) is identical to that of trivalent 2 (Figure 2, blue trace), albeit with a more cathodic open-circuit potential. Addition of $O_2$ via bubbling (10 min) leads to redox irreversibility and eventual disappearance of the original two reduction events. A new and electrochemically irreversible reduction event for the in situ generated species emerges at −1.14 V vs Fc$^+$/Fc. Infrared spectra (Figure S42) collected on samples of 1 exposed to excess $O_2$ support the notion that the divalent complex is oxidized by two electrons to form a chromyl species ([O═Cr(Ph$_2$phen)$_2$]$^{2+}$ (6)). We note that introduction of excess reducing agent (e.g., ferrocene) can regenerate the original electrochemical behavior of 1, indicating possible chemical reversibility.

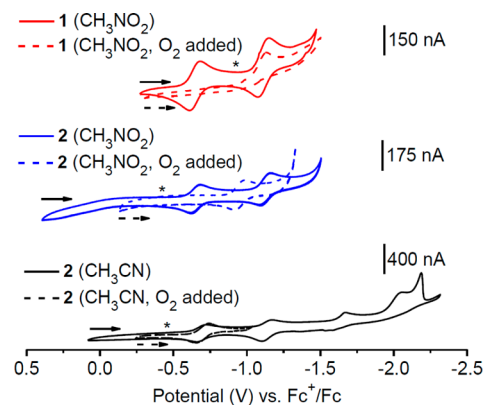For polar−aprotic solutions ($CH_3NO_2$ and $CH_3CN$) of trivalent 2, the reduction potential of the complex 3+/2+



**Figure 2.** Cyclic voltammograms (CVs) of 1 and 2, collected in 0.1 M Bu$_4$NPF$_6$ solutions with a scan rate of 100 mV/s. Solid and dashed lines represent data collected without and with oxygen bubbled through the solution, respectively. The arrows indicate the direction of the scan. The black asterisks indicate the open circuit potentials of the degassed samples. The sharp peak in the $CH_3CN$ data ($\sim$ −2.2 V) is due to a surface adsorption event that does not affect the reversibility of the system.

couple remains isovoltaic. Redox events are significantly less reversible in $CH_2Cl_2$ compared to the more polar aprotic solvents (Figure S10).

Upon addition of $O_2$ in nitromethane, the reduction potential of 2 shifts cathodically by nearly 300 mV but remains reversible (Figure 2, blue trace dashed line). We do not observe formation of a chromyl-containing species when 2 is exposed to $O_2$ via IR spectroscopy (Figure S42). Interestingly, we do not observe a similar shift in acetonitrile under the same conditions (Figure 2, black trace dashed line). We note that the larger electrochemical window for $CH_3CN$ allows us to observe reduction of oxygen to superoxide and subsequent surface chemistry. Collection of square-wave voltammograms (SWVs) while stirring alleviates some of the surface chemistry and allows us to confirm reversibility of complex-based reductions in the presence of oxygen in $CH_3CN$ (Figure S7).

To probe the effects of substrates and additives, CVs of 2 in $CH_3NO_2$ obtained under a variety of environmental conditions are presented in Figure 3. Table 1 shows the electrochemical data for the first reduction of 2 under a variety of conditions. Data from experiments performed in the dark overlap those observed under ambient light (Figures 2 and 3), with the proviso that reversibility in the "dark + $O_2$" experiment requires a glassy carbon electrode in place of a platinum working electrode, otherwise the overall peak shape changes drastically and reversibility decreases (Figure S2), suggestive of surface chemistry. Addition of the dienophile anethole (3) affords similar redox behavior to the complex alone, with and without added $O_2$. Addition of diene isoprene (4) moves the first reduction event anodically, with or without oxygen added, and removes the second reduction event. The diene is present in large excess relative to the Cr-containing complex and likely perturbs the overall electrochemical environment. Altogether, when the conditions used for the catalytic studies are probed (Table 1, entry 5), the reversibility of the first reduction of 2 in $CH_3NO_2$ is maintained at a similar potential to 2 in inert conditions (−0.64 and −0.68 V, respectively).

Analyses of electrochemical behaviors for representative alkenes (substrates and cycloadducts) provide a basis of interaction between catalyst and substrate as well as

**Table 1. Compiled Electrochemical Data for 2.**[a]

| entry | solvent (conditions)[b] | $E^0_{red}$ [Cr]$^{3+/2+}$ (V) | $E_{1/2}$ [Cr]$^{3+/2+}$ (V) | $\Delta E_p$ (mV)[c] | $E^0_{red}$ [Cr]$^{3+/2+}$ + O$_2$ (V) | $E_{1/2}$ [Cr]$^{3+/2+}$ + O$_2$ (V) | $\Delta E_p$ (mV) |
|---|---|---|---|---|---|---|---|
| 1 | CH$_3$NO$_2$ | −0.51 | −0.66 | 64 | −0.81 | −0.97 | 70 |
| 2 | CH$_3$NO$_2$ (dark) | −0.52 | −0.66 | 64 | −0.82 | −0.94[d] | 71 |
| 3 | CH$_3$NO$_2$ (+4) | −0.58 | −0.73 | 72 | −0.58 | −0.72 | 72 |
| 4 | CH$_3$NO$_2$ (+3) | −0.54 | −0.66 | 74 | −0.54 | −0.65 | 68 |
| 5 | CH$_3$NO$_2$ (+all) | −0.55 | −0.64 | 65 | −0.55 | −0.64 | 65 |
| 6 | CH$_3$CN | −0.56 | −0.68 | 69 | −0.62 | −0.73 | 167 |
| 7 | CH$_3$CN (all) | −0.59 | −0.68 | 76 | −0.59 | −0.68 | 88 |
| 8 | CH$_2$Cl$_2$ | −0.56 | −0.87 | irr. | n/a | n/a | n/a |
| 9 | CH$_2$Cl$_2$ (all) | −0.58 | −0.66 | 127 | −0.58 | −0.67 | 147 |

[a]All $E_{1/2}$ and $E^0_{red}$ values are referenced to Fc$^+$/Fc and are determined from CV data collected at 100 mV/s in 0.1 M Bu$_4$NPF$_6$ solutions in a dinitrogen atmosphere. [b]"+3" indicates addition of anethole (**3**), "+4" indicates addition of isoprene (**4**), and "+all" indicates the addition of both **3** and **4**. Additives are present at concentrations relevant to catalysis studies. [c]Values in parentheses represent separation of peak reduction and oxidation currents. [d]Experiment was performed using a glassy carbon working electrode to avoid surface chemistry.
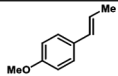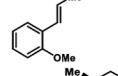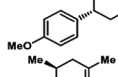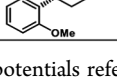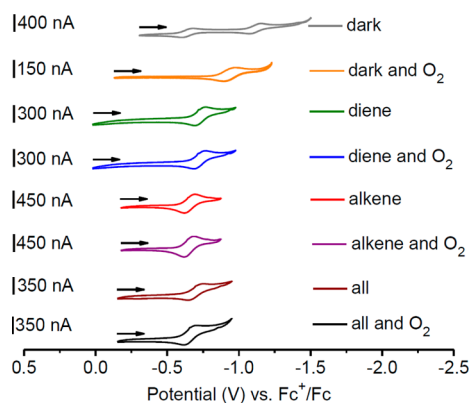


**Figure 3.** CVs of **2** obtained under several environmental conditions, collected in 0.1 M Bu$_4$NPF$_6$ CH$_3$NO$_2$ solutions with a scan rate of 100 mV/s. With the exception of the "dark" trace, the CVs focus on the first reduction event. Full scans of the experiments are available in the Figures S3−S5. The arrows indicate the open circuit potential and the direction of the scan. The data for the "dark and O$_2$" trace (blue) were collected using a glassy carbon working electrode to eliminate surface chemistry. The concentrations of the added diene (isoprene, **4**) and alkene (anethole, **3**) match those used in the catalytic studies (1:100:1000 **2**/**3**/**4**).

interactions between substrates and products (Table 2). In all cases, multiple oxidation events are observed in CVs that probe the oxidizing regime (Figures S14−37). Square-wave voltammetry allows the quasi-reversible nature of these events to be characterized. Stirred and still solutions give different reduction potentials, suggestive of surface chemistry; however, the stirred solution oxidation potentials gathered align well with literature precedent for **3**.[52] On the basis of the oxidation potentials gathered in the presence of oxygen, the only species in solution that can oxidize **3** is the excited state of Cr catalyst **2** (+0.98 V vs Fc$^+$/Fc in CH$_3$NO$_2$). Cationic compounds **3$^+$** and **5$^+$** are thermodynamically competent to oxidize anything in solution except the solvent (CH$_3$NO$_2$, CH$_3$CN) or [Cr]$^{3+}$ catalyst or **4**. Furthermore, the corresponding cycloadduct radical cations are more oxidizing than the anetholes, so they are competent to oxidize anything besides solvent, including the reduced Cr catalyst and even diene **4**.

We note that in some instances the redox potentials for the organic substrates and products measured here (Table 2) can change significantly depending on solvent and/or the presence of oxygen. The most striking changes are observed for the dienophile **3**: interestingly, the ~200 mV O$_2$-induced shift is

**Table 2. Compilation of Electrochemical Data for Methoxy-Substituted Styrenes and Cycloproducts**[a]

| compound | $E_{1/2}$ M$^{\cdot+/0}$ (V) in CH$_3$NO$_2$ | + O$_2$ | $E_{1/2}$ M$^{\cdot+/0}$ (V) in CH$_3$CN | + O$_2$ |
|---|---|---|---|---|
| (styrene, MeO-) | +0.78 | +1.00 | +1.07 | +0.86 |
| (styrene, OMe-) | +1.20 | +1.14 | +1.23 | +1.23 |
| (cyclohexene, MeO-) | +1.32 | +1.24 | +1.29 | +1.21 |
| (cyclohexene, OMe-) | +1.36 | +1.38 | +1.31 | +1.29 |

[a]All potentials referenced to Fc$^+$/Fc. All scans were performed at 100 mV/s scan rates in 0.1 M Bu$_4$NPF$_6$ solutions. O$_2$ experiments were performed by bubbling O$_2$ through the solution for ~15 s.

anodic (more oxidizing) in nitromethane but cathodic (less oxidizing) in acetonitrile. The current data might be interpreted as showing differential interactions between oxygen and organic molecules; however, further studies are required to explain this behavior, including rigorous control of [O$_2$] in the reaction. Notwithstanding, the current data show that additives (oxygen, reactants, and even solvent choice) can affect the thermodynamics of electron transfer in the cycloaddition reactions studied here.

**Spectro(-electro)chemical Studies.** Spectroelectrochemical experiments performed on **5** aim to determine the absorption characteristics of the species after oxidation (Figure S40 and S41). When this is performed free of oxygen, the absorption band at 274 nm grows upon electrochemical oxidation, whereas the transition at 225 nm remains almost the same. Additionally, the broad band centered at 991 nm decreases as the potential is increased. In the presence of oxygen, the absorption features are quite different, with only two bands of nearly equal intensity centered at 231 and 270 nm. When the potential was made more positive, no change is observed in absorption features. We conclude that different reaction pathways are available to the cycloadduct radical cation depending on the availability of oxygen; however, the exact identity of those species is not known.

The spectroscopic features of the chromyl species generated from oxidation of **1** with oxygen are presented in Figure S43. Upon full consumption of **1**, as monitored by cyclic

voltammetry, the electronic absorption spectrum of **6** shows product mixture peaks at 279 and 301 nm and a shoulder centered around 362 nm, with no absorption past 400 nm.

To probe superoxide formation, an expected side product from $^1O_2$ reduction of $[Cr]^{2+}$ to form $[Cr]^{3+}$ (Scheme 2, scenario B), several spectroscopic traps have been considered. Direct observation of $O_2^-$ under catalysis conditions is challenging because of low concentrations of the Cr-containing species and high reactivity of the cycloadduct radical cation species: performing the reaction in DMF results in product formation, but the charge transfer band attributed to a $(DMF \cdot O_2)^-$ adduct[53] is not observed. Control experiments where only **1** and **2** are present in nitromethane do show oxidation of the $[Cr]^{2+}$ in the presence of oxygen and light irradiation, without formation of a chromyl species (Figure S42). Here, although addition of superoxide traps such as TEMPOL do not show expected signals in EPR spectra for superoxide spin-trap adducts,[54−56] addition of thiophenol to the aforementioned reaction conditions results in conversion to diphenyl disulfide, indicative of the presence of superoxide (Figure S44).[40] Although these experimental results do not directly demonstrate superoxide reduction of the cycloadduct radical cation, they do establish the presence of $O_2^-$ under conditions similar to those used for the catalytic studies.

Actinometry experiments allow for the determination of quantum yields and chain lengths for the reaction of **3** and **4** in the presence of the $[Cr]^{3+}$ species **1**. Details are provided in the Supporting Information. The maximum quantum yield ($\Phi$) found is 0.35 from single wavelength excitation at 419 nm. Given a quenching factor ($Q$) of 0.99, the chain length is also 0.35, consistent with a process that does not propagate via a radical chain mechanism.

**Photophysical Studies.** Emission quenching studies of the ~750 nm phosphorescence of **2** in room-temperature $CH_3NO_2$ assist us in further understanding the relationship between the photocatalyst, substrate, and oxygen. We observe that the presence of oxygen significantly reduces the observed emission lifetime from 441 to 13 $\mu s$ upon exposure of the deoxygenated sample to atmospheric oxygen. This is readily attributed to energy-transfer quenching wherein the $^2E$ excited state of the catalyst is converted to the quartet ground state, whereas triplet oxygen is converted to its excited-state singlet.[51] We note that this observation alone might suggest that the presence of oxygen should slow down the reaction by deactivating the catalytically active $^2E$ excited state.

However, when dienophile **3** is used as the emission quencher for **2** in room-temperature $CH_3NO_2$, Stern−Volmer quenching behavior is observed for the sample in air (with ambient oxygen) as well as for a sample prepared in a dinitrogen glovebox. The results of these studies are displayed in Figure 4. As seen in both plots, the lifetime of **2** decreases upon successive addition of **3**, suggestive of reduction of the $[Cr]^{3+}$ center to $[Cr]^{2+}$ with concurrent oxidation of the alkene. The top plot corresponds to a standard Stern−Volmer analysis where the intercept is 1 and the slope is the lifetime of the molecule $\tau_0$ (inclusive or exclusive of oxygen) multiplied by the quenching rate constant $k_q$. By dividing out $\tau_0$ (bottom plot), one can remove oxygen dependence from the slope and isolate the measured dependence on anethole concentration. As can be seen from this figure, regardless of the presence of oxygen, the quenching rate constant $k_q$ is nearly identical: $9.4 \times 10^8$ $M^{-1}$ $s^{-1}$ for the degassed sample versus $9.5 \times 10^8$ $M^{-1}$ $s^{-1}$ in ambient oxygen.
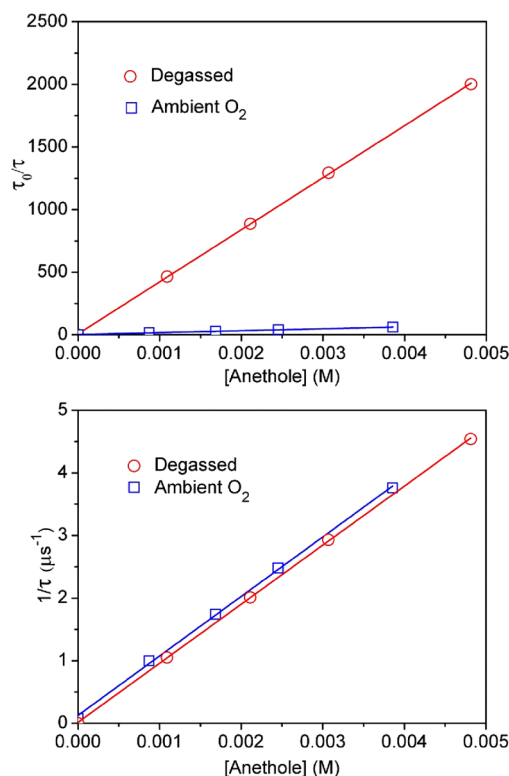


**Figure 4.** Oxygen dependence of emission quenching of **2** by **3** in room-temperature $CH_3NO_2$, showing Stern−Volmer behavior ($\tau_0/\tau$ versus quencher concentration, top) and normalized to initial lifetime ($1/\tau$ versus quencher concentration, bottom). By plotting $1/\tau$, the quenching rate constant ($k_q$) is equal to the slope: $9.4 \times 10^8$ $M^{-1}$ $s^{-1}$ degassed, $9.5 \times 10^8$ $M^{-1}$ $s^{-1}$ ambient $O_2$. The data are fit to a linear function using least-squares methodology.

The reaction of **3** and **4** with catalytic **2** in nitromethane, monitored by electronic absorption spectroscopy, shows significant differences as a function of oxygen presence. In the oxygen-free experiment, significant spectral changes are observed. These are plotted as a difference spectrum in Figure 5. This spectral shape grows monotonically over time and does not appear to contain unrelated features. We can replicate the salient features as the creation of 1 equiv of divalent **1** for the loss of every 5 equiv of trivalent **2**. A brown solid precipitates over the course of the experiment, which is likely to be a reduced chromium degradation product due to the enhanced
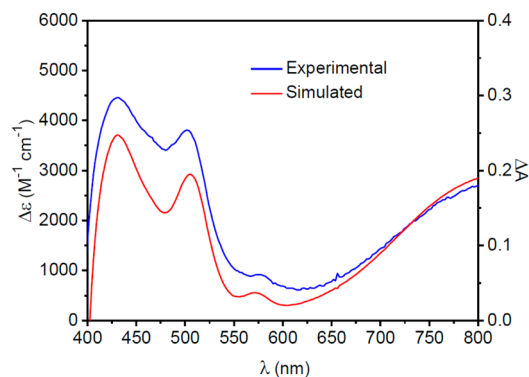


**Figure 5.** Electronic absorption difference spectrum after a 40 h photoreaction in which oxygen was excluded and a simulated spectrum consisting of the growth of **1** and loss of **2** in a 1:5 ratio.

## Table 3. Computed Reaction Energetics (kcal/mol)

| reaction | $\Delta TE^a$ | $\Delta H_r^{\ b}$ | $\Delta G_r^{\ c}$ |
|---|---|---|---|
| $3 + 4 \rightarrow 5$ | −48.0 | −44.1 | −28.4 |
| $^22(BF_4)_3 + 3 \rightarrow {}^31(BF_4)_2 + {}^23 \cdot BF_4$ | −4.5 | −6.0 | −7.8 |
| $^22(BF_4)_3 + 4 \rightarrow {}^31(BF_4)_2 + {}^24 \cdot BF_4$ | 12.6 | 10.4 | 7.4 |
| $^42(BF_4)_3 + 3 \rightarrow {}^31(BF_4)_2 + {}^23 \cdot BF_4$ | 35.3 | 33.8 | 32.0 |
| $3 + {}^1\Delta O_2 + TMA \cdot BF4 \rightarrow {}^23 \cdot BF_4 + {}^2O_2 \cdot TMA^d$ | 20.0 | 20.6 | 20.5 |
| $^23 \cdot BF_4 + 4 \rightarrow {}^23 \cdot BF_4 \cdot 4$ | −9.7 | −8.3 | 2.7 |
| $^23 \cdot BF_4 \cdot 4 \rightarrow [^23 \cdot BF_4 \cdot 4] \ TS^e$ | 1.3 | 1.0 | 4.3 |
| $^31(BF_4)_2 + {}^25 \cdot BF_4 \rightarrow {}^42(BF_4)_3 + 5$ | −42.3 | −40.8 | −38.5 |
| $^31(BF_4)_2 + {}^3O_2 + TMA \cdot BF_4 \rightarrow {}^42(BF_4)_3 + {}^2O_2 \cdot TMA$ | 5.7 | 7.8 | 9.5 |
| $^31(BF_4)_2 + {}^1\Delta O_2 + TMA \cdot BF_4 \rightarrow {}^42(BF_4)_3 + {}^2O_2 \cdot TMA$ | −15.2 | −13.2 | −11.5 |
| $^25 \cdot BF_4 + {}^2O_2 \cdot TMA \rightarrow 5 + {}^3O_2 + TMA \cdot BF4$ | −48.0 | −48.6 | −48.0 |
| $^23 \cdot BF_4 + {}^3O_2 \rightarrow {}^23 \cdot BF_4 \cdot O_2 \ (superoxo)$ | −4.9 | −2.7 | 8.7 |
| $^23 \cdot BF_4 + {}^3O_2 \rightarrow {}^23 \cdot BF_4 \cdot O_2 \ (dioxetane)$ | −3.3 | −1.2 | 11.7 |
| $2 \ {}^23 \cdot BF_4 \rightarrow (^23 \cdot BF_4)_2$ | −32.3 | −29.0 | −12.1 |
| $2 \ {}^23 \cdot BF_4 + {}^3O_2 \rightarrow (3 \cdot BF_4)_2 O_2$ | −44.6 | −39.6 | −13.5 |
| $^25 \cdot BF_4 + {}^3O_2 \rightarrow {}^2product \cdot BF_4 \cdot O_2 \ (superoxo)$ | 6.9 | 7.3 | 19.4 |
| $^25 \cdot BF_4 + {}^3O_2 \rightarrow {}^2product \cdot BF_4 \cdot O2 \ (superoxo) \ TS$ | 10.4 | 9.9 | 21.7 |
| $^25 \cdot BF_4 + {}^3O_2 \rightarrow {}^2product \cdot BF_4 \cdot O_2 \ (dioxetane)$ | −18.1 | −15.7 | −2.6 |
| $5 + {}^3O_2 \rightarrow product \cdot O_2 \ (dioxetane)$ | −19.3 | −16.8 | −4.1 |
| $^25 \cdot BF_4 + 3 \rightarrow product + {}^23 \cdot BF_4$ | −7.0 | −7.0 | −6.5 |
| $^25 \cdot BF_4 + 4 \rightarrow {}^25 \cdot BF_4 \cdot 4$ | −10.8 | −9.3 | 2.5 |
| $^25 \cdot BF_4 \cdot 4 + 3 \rightarrow 5 \cdot 4 + {}^23 \cdot BF_4$ | −2.3 | −2.4 | −4.4 |

$^a\Delta TE$ is the difference in total energies. $^b\Delta H_r$ adds zero point and heat capacity effects. $^c\Delta G_r$ adds the entropic contribution. $^d$TMA is tetramethylammonium ion. $^e$TS is transition state.

## Scheme 5. Computed Reaction Pathways$^a$
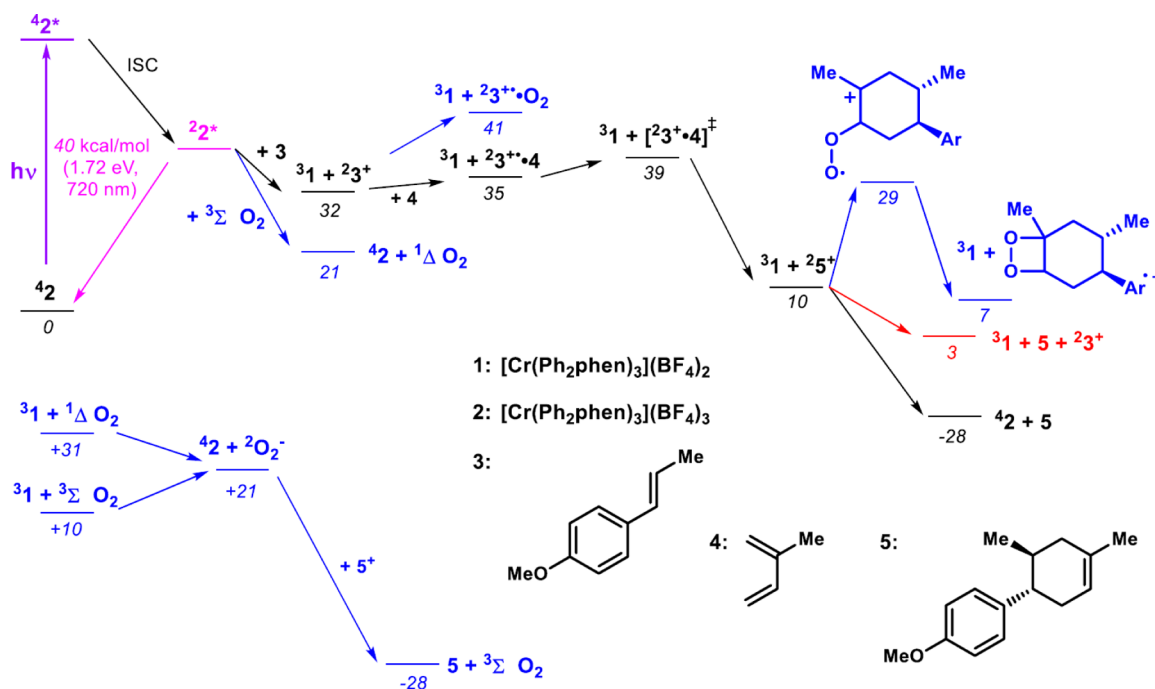


$^a$The top scheme considers all processes related to Scheme 2; the bottom scheme considers energetics associated with superoxide formation as part of catalyst regeneration. Blue entities represent possible routes affected by oxygen-containing species; the red route represents species involved in radical chain events. Free energies (in italics) are provided as kcal/mol relative to the ground state of the photocatalyst **2**.

lability of the divalent species relative to the bona fide [Cr]$^{3+}$ complex. In contrast, in the presence of oxygen, the loss of **2** is observed with no concurrent growth in features attributable to **1** (Figure S46) and without any appearance of an insoluble brown solid. Changes in relative absorbances (i.e., not solely

loss of **2**) in the visible region are responsible for the darkening of the solution, consistent with some decomposition of Cr-containing catalyst and/or emergence of absorptive radical cations (Figures S48 and S50).

**Electronic Structure Calculations.** Density functional electronic structure theory provides energetic corroboration for the various experimental observations. Results are collected in Table 3 and summarized in Scheme 5.

As with most Diels−Alder reactions, wherein three $\pi$ bonds are converted into two $\sigma$ bonds and a $\pi$ bond, the process is significantly exoergic, computed to be downhill by 28 kcal/mol. The doublet excited state of **2**, $^2$**2**, is computed to be thermodynamically competent to oxidize **3**, generating a radical cation, $^2$**3**·BF$_4$, 8 kcal/mol exoergic, whereas for the quartet ground state, the reaction is 32 kcal/mol endoergic. Oxidation of the diene, **4**, by $^2$**2** is computed to be 7 kcal/mol endoergic. Diene **4** is computed to bind to $^2$**3**·BF$_4$ as a $\pi$ complex with a binding enthalpy of 10 kcal/mol but with an endoergic free energy of 3 kcal/mol. The $^2$**3**·BF$_4$·**4** $\pi$ complex is computed to proceed toward product with an electronic barrier of only 1 kcal/mol relative to the $\pi$ complex. The free energy of activation is 4 kcal/mol. The reduced chromium complex $^3$**1** thermodynamically can reduce the oxidized cycloadduct product radical cation, $^2$**5**·BF$_4$. Oxidation of $^3$**1** by $^3$O$_2$ is computed to be endothermic by nearly 6 kcal/mol, whereas reaction with $^1\Delta$O$_2$ is exothermic by 15 kcal/mol with an exoergicity of 12 kcal/mol. Reduction of $^2$**5**·BF$_4$ by superoxide is computed to be 48 kcal/mol exothermic. Oxidation of **3** by $^1\Delta$O$_2$ is computed to be 21 kcal/mol endoergic.

The dienophile anethole, **3**, is observed to quench $^2$**2**. The triplet excited state of **3** is computed to be 74 kcal/mol (vertical, 60 kcal/mol adiabatic) above the ground state, whereas $^2$**2** is at 39 kcal/mol. Oxidation of **3** by $^2$**2** is 4 kcal/mol exothermic, whereas reduction of $^2$**3**·BF$_4$ by $^3$**1**(BF$_4$)$_2$ is 35 kcal/mol exothermic.

To investigate whether $^3$O$_2$ is thermodynamically competent to stabilize $^2$**3**·BF$_4$ or the resultant $^2$**5**·BF$_4$, superoxo and dioxetane radical cation structures were computed. Both superoxo and dioxetane isomers are computed to be slightly exothermic but significantly endoergic for $^2$**3**·BF$_4$, 9 and 12 kcal/mol, respectively. For $^2$**5**·BF$_4$ superoxide formation is endoergic by 19 kcal/mol, whereas radical cation dioxetane formation is 3 kcal/mol exoergic. The saddlepoint for $^2$**5**·BF$_4$ superoxide formation is 22 kcal/mol endoergic (3 kcal/mol above the intermediate).

To contribute to our understanding of the electrochemistry, the radical cation dimer of **3** was studied along with the analogous dimer peroxide: these species were found by Bard and co-workers to be formed electrochemically.[31] Both dimeric complexes were computed to be exoergic, by 12 and 14 kcal/mol, respectively.

Finally, to investigate whether a radical chain process is viable, reduction of **3** by $^2$**5**·BF$_4$ was considered. The process was computed to be 7 kcal/mol exoergic.

The computed electronic spectra of $^3$**1**(BF$_4$)$_2$, $^4$**2**(BF$_4$)$_3$ **3**, $^2$**3**·BF$_4$, **5**, and $^2$**5**·BF$_4$ are provided in Figures S47−S52. Net spin density plots for $^3$**1**(BF$_4$)$_2$, $^4$**2**(BF$_4$)$_3$, $^2$**3**·BF$_4$, $^2$**5**·BF$_4$, and the superoxo and dioxetane isomers of $^2$**3**·BF$_4$·O$_2$ and $^2$**5**·BF$_4$·O$_2$ are also provided in Figures S53−57, S60, S63, and S65. Finally, electrostatic potentials mapped onto the total electron density are provided for the superoxo and dioxetane isomers of $^2$**3**·BF$_4$·O$_2$ and $^2$**5**·BF$_4$·O$_2$ in Figures S58, 59, 61, 62, 64, and 66.

## ■ DISCUSSION

As outlined in the introduction, the observed photocatalytic coupling of anethole (**3**) with isoprene (**4**) mediated by [Cr(Ph$_2$phen)$_3$](BF$_4$)$_3$ (**2**) requires the presence of oxygen.

Data relevant to the catalytic cycle and several potential roles for O$_2$ have been considered and are discussed in light of the results presented above.

Before proceeding, a comment on measured electrochemical potentials is warranted by their importance in designing (photo)redox catalytic schemes and choosing "viable" reactants. From a strictly thermodynamic standpoint, the feasibility of an electron transfer event depends on the electrochemical onset potential ($E^0_{red/ox}$). This quantity is also directly related to the results of electronic structure computations. However, in a complex catalytic system, especially photoredox systems, the rate of electron transfer also matters because it affects the concentrations of key intermediates that may be involved in (nonredox) processes downstream. Practically, $E_{1/2}$ reduction potentials are considered to be more applicable because they are related to the peak currents produced in the redox event and thus generally indicate fast-enough kinetics. Notwithstanding, slow kinetics may prevent a key intermediate from being produced in an otherwise thermodynamically competent reaction; conversely, an irreversible process subsequent to electron transfer may allow a reaction to proceed where the $E_{1/2}$ values might suggest thermodynamic incompetence.

Both thermodynamics and kinetics of electron transfer are affected by changes in local environment. Unfortunately, we find several examples of recent photocatalysis literature that report reduction potentials without reference to solvent and other environmental conditions. It is well known that reduction potentials can vary greatly depending on solvent: for instance, Ag$^+$/Ag reduction is +40 mV in acetonitrile but +650 mV in dichloromethane (both vs Fc$^+$/Fc).[57,58] Related, several photoredox catalysis reactions afford good yields only in uncommon solvents such as 1,3-dimethyl-2,4,5,6-tetrahydro-2(1H)-pyrimidinone (DMPU) or trifluoroethanol.[59,60]

Given this context, we investigated the reduction potential of **2** under several conditions to quantify the relative impacts on a key step in the catalytic process. Our original goal was to measure these potentials in environments matching as closely as possible the catalysis conditions in operando. Depending on the additives (substrates and/or O$_2$), we observe that the $E_{1/2}$ value for **2** changes by up to 330 mV and that reversibility is not always maintained. When substrates and/or oxygen are present, we find that the shifts in reduction potentials (Figure 3) appear to be dominated by the diene (**4**), which is present in 1000-fold excess relative to the catalyst **2**. Here, the electrolyte is an important perturbation because the concentration of O$_2$ is salt-dependent: for example [O$_2$] is decreased by a factor of ∼2 when salt is present in acetonitrile.[29] Unfortunately, these electrochemical experiments are not possible without a salt present. Besides $E_{1/2}$ values, the difference in peak oxidation and reduction currents ($\Delta E_p$) provides some indication of how electron transfer rates are modulated by the additives. For instance, under dinitrogen the $\Delta E_p$ values for **2** and **2** + **3** are 64 and 74 mV, respectively (Table 1), indicating slower kinetics for the latter even though the thermodynamics remain constant ($E_{1/2}$ = −0.66 V).

Key findings from this exploration are as follows. First, the catalyst shows varied reduction potentials in nitromethane with and without oxygen added, but once substrates **3** and **4** are included, the reduction potential is quite similar to that measured under oxygen-free conditions. Second, the catalyst reduction potentials are similar in different solvents when both substrates and oxygen are present, but the decrease in peak potential difference suggest that the kinetics of electron transfer

are a little faster in nitromethane than in acetonitrile. Finally, although measurement of electrochemical properties in operando is a good target, here $[O_2]$ is difficult to control experimentally and intractable to follow computationally; in these cases it is better to use the potentials generated from pristine conditions where all additives (especially $O_2$ here) can be controlled.

**Excitation of Cr-Catalyst.** The reaction is initiated by visible or near-UV light excitation of the Cr catalyst to what is thought to be a charge transfer transition ($^4CT \leftarrow {}^4A$), followed by nonradiative decay including intersystem crossing into a lower-energy, long-lived $^2E$ state. The photochemistry can occur from this state because it persists on a microsecond time scale, well beyond the time required to diffuse in solution and interact with a substrate. Alternatively, the catalyst can phosphoresce from this same state with a maximum intensity at 750 nm, well outside of the absorbing region. This provides a suitable signal for investigating the excited state behavior of the catalyst in the present system, which has been studied previously.[32,61] Oxygen is observed to quench this doublet excited state through an energy transfer pathway, reducing the amount of photoexcited catalyst and slowing down the overall reaction but not inhibiting it. This quenching event also results in the formation of singlet oxygen.[51]

**Oxidation of Dienophile and Subsequent Cyclization.** The $^2E$ excited state of the chromium catalyst **2** is energetically competent to oxidize the dienophile **3**, computed to be 8 kcal/mol exoergic, whereas electrochemical ($E_{1/2}$) potentials suggest thermoneutrality. Electrochemical data (Figures 2 and 3) collected on reactants **3** and **4** and catalyst **2** further validate the computations (Figures S51 and S52). The observed quenching behavior in Figure 4 supports the kinetic viability of the process. Given the energetic inaccessibility of the dienophile triplet excited state, quenching likely occurs via electron transfer from the dienophile to the chromium complex, followed by either back electron transfer from chromium to the dienophile radical cation or dissociation of the radical cation. Here, the catalytically productive process (dissociation) can be favored by cation–cation repulsion because the photoreduced chromium complex is still divalent. The rate of the excited state quenching event involving **2\*** and **3** is almost identical in and out of the presence of oxygen, confirming that oxygen does not play a significant role in dienophile oxidation. Furthermore, as demonstrated in Figure 5, under photolysis conditions but without oxygen, the catalyst **2** is reduced to **1**.

Experimentally, we find that final product formation is not observed in the absence of chromium, confirming that oxygen alone is not able to perform this reaction. Oxidation of the dienophile **3** by $^1\Delta O_2$ is computed to be 21 kcal/mol endoergic; this reaction is even more unfavorable if ground-state $^3O_2$ is used. Furthermore, singlet oxygen has an oxidation potential of −0.44 V vs Fc$^+$/Fc, which makes it unable to oxidize **3** in nitromethane with $O_2$ present ($E_{1/2}$ = +1.00 V vs Fc$^+$/Fc corresponds to a free energy difference of 33 kcal/mol). Oxidation of the diene is also not observed in any reactions because this is not thermodynamically accessible by **2**, whether in ground or excited states. Oxidation of isoprene is computed to be 7 kcal/mol endoergic. $E_{1/2}$ data also suggest a 7 kcal/mol endoergicity.

We note that mono-oxidized *para*-anethole **3**$^+$ is reported to electrochemically dimerize,[31] but we do not observe this reaction under the standard reaction conditions used for the

catalysis studies. Even though the reaction involves two cations combining to form a dication, we compute the radical cation dimerization reaction of $^2$**3**·BF$_4$ to be 12 kcal/mol exoergic in acetonitrile, consistent with what was observed previously by Demaille and Bard.[31] Reaction of two equivalents of $^2$**3**·BF$_4$ with $^3O_2$ is computed to be 13 kcal/mol exoergic. Despite favorable thermodynamics, dimerization is not observed within reasonable limits of detection under our photocatalytic conditions, likely due to a concentration effect. Electrochemically, the concentration of anethole radical cation builds up near the electrode to promote dimerization, whereas under chemical oxidation or photocatalytic oxidation conditions the radical cation is dispersed throughout the solution at low concentration. Dating to the 1970s, such anodic chemistry has proven challenging for dienes and dienophiles.[33,62−64]

An alternative role for oxygen in the mechanism is to stabilize the dienophile radical cation **3**$^+$ so that it has sufficient lifetime to find a diene in solution. However, we compute the formation of end- or side-on (dioxetane) oxygen complexes with **3**$^+$ to be endergonic (Table 3), and we do not observe these species spectroscopically. In addition, the similar initial rate constants observed in the quenching of **2\*** by **3** with and without oxygen present do not support formation of an intermediate species.

Radical cyclization involving **3**$^+$ and **4** to form **5**$^+$ should be, and is computed to be, nearly barrierless. The 10-fold excess of diene utilized in catalysis conditions favors anethole radical cation reaction with a diene rather than with another dienophile. Thus, we conclude that oxygen does not play a significant role in the oxidation of the dienophile and subsequent cyclizations with alkenes.

**Regeneration of the Cr Catalyst.** Under catalytic conditions but absent $O_2$, the loss of ∼80% of the trivalent Cr complex **2** signal suggests that the excited state complex is prone to decomposition, most likely from ligand loss and/or solvent incorporation, as described previously.[27] Related, buildup of the divalent Cr species **1** (Figure 5) indicates that the radical cyclo-intermediate, $^2$**5**$^+$, does not succeed overall as an oxidant and cannot return the catalyst to the bona fide 3+ oxidation state, even though it is thermodynamically competent to do so. The computed exoergicity of that reaction is 39 kcal/mol, and the electrochemistry of the two species suggest favorable reactivity ($E_{1/2}$ data suggest a 43 kcal/mol exoergicity). However, no product is formed without oxygen, so the kinetics of the air-free route must be relatively slow. Possible explanations for this nonevent are as follows: first, the diffusion rates of large ionic species are expected to be dramatically slower than those of oxygen and redox congeners (e.g., superoxide); separately or in conjunction, cation–cation repulsion may prevent radical cation approach to the photoreduced [Cr]$^{2+}$ complex.[65,66]

Related, we do not believe that a chromyl species (formed when divalent **1** is exposed to excess oxygen bubbled through solution) is actively involved in the regeneration of the catalyst. We observe spectroscopic evidence for this species only when the divalent complex **1** is exposed to oxygen, not when the trivalent complex **2** is used. In addition, we do not observe a chromyl species under conditions when diene and dienophiles are present in the reaction mixture. The oxidized species has no significant absorptions in the visible spectrum where the highest overall reaction yields are obtained. Finally, any mechanism in which chromyl participation is invoked requires a two-electron oxidation and diimine ligand (here, Ph$_2$phen) dissociation to form the species, followed by one electron reduction and ligand

**Scheme 6. Proposed Catalytic Cycle**
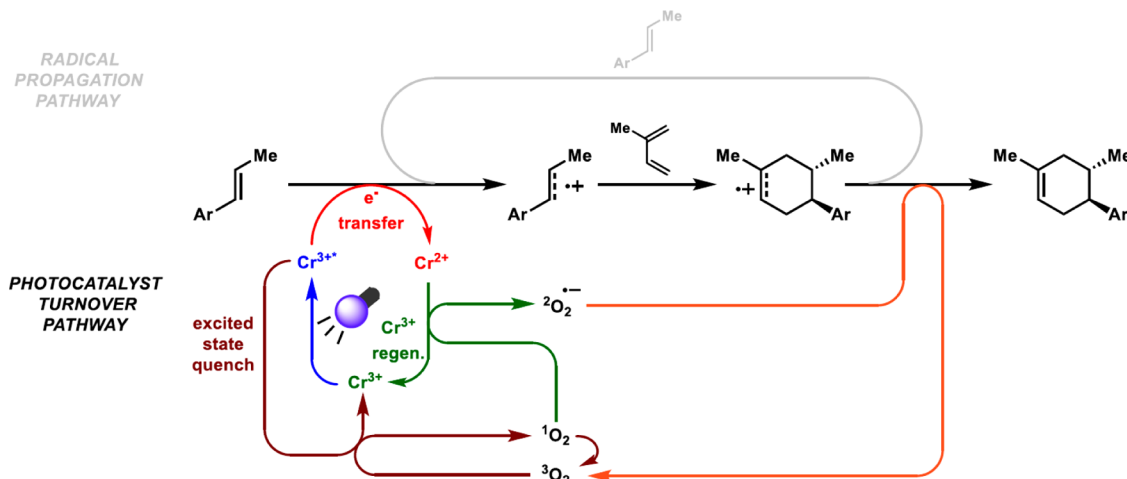


reassociation. Although not impossible,[67] given the dilute nature of the Cr-containing complexes in solution, the polar solvents used, and the overall slow kinetics, we would expect the required ligand binding events are unlikely to occur in this catalytic cycle.

On the basis of the combined experimental and computational studies, we hypothesize that regeneration of **2** comes in two forms. First, ground-state oxygen ($^3\Sigma O_2$) can quench the excited state **2***; this produces singlet oxygen ($^1\Delta O_2$) and likely prevents ligand loss in the Cr-containing complex. Second, $^1\Delta O_2$, formed from the observed quenching of the photoexcited $^2$**2** species, returns the catalyst to its 3+ oxidation state and forms superoxide in the process.

**Reduction of the Cycloadduct Radical Cation.** Considering species in solution that could reduce the radical cation cycloadduct to the final product **5**, the photoreduced Cr catalyst **1** is competent to reduce **5**$^+$ directly. In addition, dienophile **3** is both computationally and electrochemically capable of reducing **5**$^+$ and thus could participate in a radical chain pathway. However, we observe minimal product (**5**) formation when oxygen is excluded from the reaction mixtures, consistent with the idea that neither the reduced catalysts nor dienophiles are efficient electron shuttles in this system even though the former are easily photogenerated and the latter are present in large concentration relative to cycloadduct cations formed.

The principal role of an oxygen-containing species is difficult to observe directly. Although the radical cation **5**$^+$ is not sufficiently stable to interrogate directly, spectroelectrochemistry experiments performed on **5** show different radical cation species depending on the availability of oxygen. In related systems, cyclic alkylperoxides have been proposed and isolated previously after oxidation of oxidatively reactive substrates.[68,69]

However, despite favorable thermodynamics and literature precedent, neither dioxetanes nor the products of transient dioxetane formation are observed under photocatalytic conditions. Once formed, dioxetanes are known to fragment, forming aldehyde or ketone cleavage products.[68] For cycloaddtion product **5**, the radical cation dioxetane is computed to be 3 kcal/mol exoergic relative to the radical cation. Furthermore, the subsequently reduced dioxetane is 3 kcal/mol exoergic relative to the observed product and $^3O_2$. Plausible formation of the dioxetane radical cation involves the intermediacy of a superoxo complex. The net spin density

plots of the radical cations of anethole (Figure S53) and the cycloadded product (Figure S54) suggest that the radical is stabilized by/localized on the aromatic ring. For the cycloaddition product the spin density is completely localized on the aromatic ring. Reaction with $^3O_2$ requires relocalization of the spin onto the isolated double bond in the product (Figures S58, 61, 64, and 66). The superoxide intermediate is 19 kcal/mol endoergic, relative to the radical product and $^3O_2$, and the saddlepoint was another 3 kcal/mol above the intermediate.

Given the considerations listed above and the fact that oxygen is necessary for the reaction to proceed, we hypothesize that an oxygen-containing species acts as the electron transfer agent for the last step of the catalytic cycle. Superoxide is thermodynamically competent to reduce the product cyclohexenyl radical cation: the $O_2/O_2^-$ couple in acetonitrile is −1.42 V vs Fc$^+$/Fc,[29,30] whereas the **5**$^+$/**5** couple is centered at +1.3 V (suggesting a 63 kcal/mol exoergicity). The computed exoergicity of the reaction is 48 kcal/mol. In contrast to the reaction of reduced catalyst **1** with **5**$^+$, where charge−charge interactions are repulsive, here there is an electrostatic attraction between the negatively charged superoxide and **5**$^+$, and the approach of radicals is likely near barrier-free.

Amassing direct evidence of cycloadduct radical cation reduction by superoxide in operando is challenging because of the low concentrations and high reactivities of the two species. One piece of indirect evidence is the significantly lower product yield for reactions performed in the presence of benzoquinone, a known superoxide scavenger,[70] consistent with inhibition of superoxide. In addition, the reaction quantum yield determinations are not consistent with radical chain propagation, suggesting that a species other than the dienophile **3** is responsible for generating new radical cations.

More directly, photoirradiation of oxygenated solutions of **1** and **2** (without other organic reactants) results in the oxidation of all [Cr]$^{2+}$ to [Cr]$^{3+}$ without formation of chromyl species, consistent with $^1O_2$ consumption. The superoxide presumably formed by concomitant reduction of singlet oxygen is not detected spectroscopically using either TEMPOL (a spin-trap) or DMF (a charge-transfer trap) presumably because of slow kinetics of formation in nonaqueous media in the former case and weak binding interactions in the latter. However, addition of thiophenol to the photoirradiated mixture results in the rapid formation of diphenyl disulfide, as observed via $^1$H NMR spectroscopy; this has been employed recently as a reporter

reaction for the detection of superoxide.[40] Thus, although the reaction of superoxide with **5**[+] is not directly observed, there is strong evidence for presence of superoxide in the catalytic system and its potential to interact with an organic substrate.

**Overall Catalytic Cycle Including Oxygen.** Our current understanding of the Cr-mediated cycloaddition catalytic cycle is provided in Scheme 6. Oxygen appears to protect the Cr catalyst by quenching the excited state when substrate (dienophile) is not immediately available; it also oxidizes the [Cr]²⁺ species to regenerate the catalyst. Finally, it shuttles electrons to the cycloadduct cation (as superoxide) to produce the final product.

In principle, oxygen's roles in this Cr-catalyzed system form closed cycles in which there is no net change in oxygen concentration and/or buildup of oxygen-containing (photo)-redox side products. In practice, the efficiency of intermediate formation, for example, superoxide, which appears to be the key player in final product formation, should depend heavily on the relative concentrations of singlet oxygen, Cr catalyst and light, and also the stability of the oxidized dienophile. Imbalance in any of these concentrations could overexpress superoxide, leading to incorporation into cyclized products; alternatively, insufficient superoxide should slow product formation and/or activate a radical chain pathway, both of which could lead to lower yields and/or loss of stereochemical control. As shown in Scheme 4, yields for different substrates may be affected by relative concentrations of $O_2$, reflective of this delicate balance; further studies probing concentration effects are in progress. We note that all of the relevant species are present in solution in comparable (mM) concentrations.[71] In addition, Cr excited state quenching by oxygen and substrate are competitive;[72] excited state lifetimes for the catalyst and $^1\Delta O_2$ (13 and 40 $\mu s$, respectively) are also comparable. It is rather amazing that this catalytic cycle works. Notwithstanding, this seemingly fortuitous catalytic cycle presents an efficient means to perform photocatalytic reactions.

**Comparison of Ru- and Cr-Based Photoredox Catalysis.** At this juncture, it is reasonable to compare the present Cr-catalyzed system **2** to the literature $[Ru(bpz)_3]^{2+}$ photoredox system. Comparative data is collected in Table S1.[73,74] In acetonitrile, the excited state reduction potentials for $[Ru(bpz)_3]^{2+*/1+}$ and $[Cr(Ph_2phen)_3]^{3+*/2+}$ are nearly identical (~1 V vs Fc⁺/Fc). The excited state lifetime is significantly shorter for the Ru complex than for the Cr species, even if the quenching effects of oxygen are included (<0.9 and 13 $\mu s$, respectively). The ground state reduction potentials for both $[Ru(bpz)_3]^{2+/1+}$ and $[Cr(Ph_2phen)_3]^{3+/2+}$ in $CH_3CN$ are such that neither of the reduced forms of these catalysts should be oxidized by $^3O_2$ (the Ru complex is much closer), but both are competent to reduce the cycloaddition product radical cation. Interestingly, however, neither appears to do so. Absent $O_2$, a 48% yield of **5** is reported for the $[Ru(bpz)_3]^{2+}$-containing system; whereas for **2**, only trace amounts of **5** are observed. This difference is consistent with minimal photocatalyst turnover for each, but with Ru serving as an initiator for a radical chain (with a radical chain length of roughly 50), whereas Cr only produces approximately stoichiometric product.[39] Reported $^3O_2$ quenching rates for excited states in the related complexes $[Ru(bpy)_3]^{2+}$ and $[Cr(bpy)_3]^{3+}$ are 6.8 × 10⁸ and 2.5 × 10⁷ $M^{-1}$ $s^{-1}$, respectively, in acetonitrile.[75,76] Wrighton and Markham have reported competitive oxygen and aryl alkene quenching in Ru-based systems,[77,78] comparable to our observation of competitive quenching by dienophile and

oxygen in a Cr-based system. In general, for each photophysical process Ru is faster and/or has a shorter lifetime than the Cr complex studied here.

We note that one additional point of divergence is solvent choice. Optimal product yields are obtained in nitromethane for the Cr-based system and dichloromethane for the Ru-initiated process. Performing the reaction of interest in dichloromethane leads to an overall lower yield compared to nitromethane (50 vs 88% respectively), and we observe no significant change in overall reaction rates. At this time, we cannot rule out differential interactions between solvent and reactants or intermediates, but the data collected thus far suggest that solvent choice does not switch the dominant mechanistic pathway observed.

Regarding oxygen's influence, Yoon and co-workers observed endoperoxide product formation in the $[Ru(bpz)_3]^{2+}$-mediated oxidative cyclization of bis(styrenyl) substrates under standard photocatalytic conditions.[79] The formation of this product is predominant when increasing the oxygen concentration (via headspace pressure) from 1 to 4 atm. The authors proposed that the initially formed radical cation was intercepted by triplet oxygen, forming an endoperoxide radical cation.[79] From this result it is clear that oxygen can be involved directly in the reaction sequence, and relatively small changes in experimental conditions can alter final product distributions.

On the basis of these observations and assembled data, we suggest that $[Ru(bpz)_3]^{2+}$ and $[Cr(Ph_2phen)_3]^{3+}$ (**2**) likely follow a common catalytic cycle, comparable to what is shown in Scheme 6, where relatively small deviations in rates and lifetimes favor the radical chain mechanism for the Ru complex but oxygen-mediated photocatalysis for the Cr complex. Because the excited states of Ru-containing complexes react more quickly with organic substrates (by approximately a factor of 10), this arguably increases the concentration of cycloadduct radical cation in the reaction mixture, which in turn favors the radical chain pathway. Meanwhile, the longer excited state lifetime of the Cr complex offers more opportunities for energy transfer to $^3O_2$ to produce $^1O_2$. Here, a larger buildup of $^1O_2$ ultimately leads to a higher concentration of superoxide, which in turn reduces the concentration of cycloadduct radical cation by reduction. This lower concentration of cycloadduct radical cation deactivates the radical chain pathway. Kinetic models that test these ideas are being constructed and will be reported at a later date.

## ■ CONCLUSIONS AND OUTLOOK

The Cr-photocatalyzed Diels−Alder reaction between anethole and isoprene has been investigated with a range of tools with the goal of refining the reaction mechanism, specifically defining the critical role(s) that oxygen plays in this catalytic cycle and perhaps others. We observe a direct interaction between the long-lived (²E) Cr(III) excited state and dienophile, supporting the previously reported mechanistic hypothesis that the Cr excited state directly participates in anethole oxidation. Furthermore, from the buildup of **1** under catalytic conditions absent $O_2$ (Figure 5), we conclude that even though thermodynamically competent the cycloaddition product radical cation is not kinetically competent to directly oxidize the reduced Cr catalyst. We observe that ²E Cr(III) excited state quenching by oxygen and anethole are competitive processes but follow orthogonal paths. Oxygen quenching does not shut down the catalytic cycle; in fact, it appears to be critical for catalyst stability and therefore catalytic turnover. We

support the previous observation that oxygen does not play the deleterious role of oxidizing the organic substrates or product; rather, we suggest that it serves as an electron shuttle, through the intermediacy of superoxide, between the reduced Cr catalyst and the oxidized cycloaddition product.

The results presented herein provide insight into oxygen's participation as a sustainable reagent in photoredox catalysis. The results also support the proposition that long-lived excited states in Cr(III) complexes can make available mechanistically distinct pathways from processes initiated by heavier congeners (e.g., Ru and Ir). These alternative reaction pathways could be exploited to achieve orthogonal reactivity. At the same time, the divergent reaction sequences are likely accessible to both heavy and light transition metal complexes, and small changes in environmental conditions may allow switching between radical chain and photocatalytic pathways. Our current and future efforts aim to parametrize the kinetic and thermodynamic quantities involved in this oxygen-mediated mechanism so as to optimize reaction scope and control product structure.

## ■ ASSOCIATED CONTENT

### Ⓢ Supporting Information

The Supporting Information is available free of charge on the ACS Publications website at DOI: 10.1021/jacs.6b02723.

Details of experimental procedures, supplementary electrochemical data, computed data, and spin density plots. (PDF)

## ■ AUTHOR INFORMATION

### Corresponding Authors
*E-mail: anthony.rappe@colostate.edu.
*E-mail: matthew.shores@colostate.edu.

### Notes
The authors declare no competing financial interest.

## ■ ACKNOWLEDGMENTS

## ■ REFERENCES

(1) Prier, C. K.; Rankic, D. A.; MacMillan, D. W. C. *Chem. Rev.* **2013**, *113*, 5322.
(2) Xuan, J.; Xiao, W.-J. *Angew. Chem., Int. Ed.* **2012**, *51*, 6828.
(3) Narayanam, J. M. R.; Stephenson, C. R. J. *Chem. Soc. Rev.* **2011**, *40*, 102.
(4) Yoon, T. P.; Ischay, M. A.; Du, J. *Nat. Chem.* **2010**, *2*, 527.
(5) Beatty, J. W.; Stephenson, C. R. J. *Acc. Chem. Res.* **2015**, *48*, 1474.
(6) Lin, S. S.; Ischay, M. A.; Fry, C. G.; Yoon, T. P. *J. Am. Chem. Soc.* **2011**, *133*, 19350.
(7) Stevenson, S. M.; Shores, M. P.; Ferreira, E. M. *Angew. Chem., Int. Ed.* **2015**, *54*, 6506.
(8) Ventre, S.; Petronijevic, F. R.; MacMillan, D. W. C. *J. Am. Chem. Soc.* **2015**, *137*, 5654.
(9) Zuo, Z.; Ahneman, D. T.; Chu, L.; Terrett, J. A.; Doyle, A. G.; MacMillan, D. W. C. *Science* **2014**, *345*, 437.
(10) Noble, A.; McCarver, S. J.; MacMillan, D. W. C. *J. Am. Chem. Soc.* **2015**, *137*, 624.
(11) Bock, C. R.; Meyer, T. J.; Whitten, D. G. *J. Am. Chem. Soc.* **1974**, *96*, 4710.
(12) Meyer, T. J. *Acc. Chem. Res.* **1989**, *22*, 163.
(13) Gualandi, A.; Marchini, M.; Mengozzi, L.; Natali, M.; Lucarini, M.; Ceroni, P.; Cozzi, P. G. *ACS Catal.* **2015**, *5*, 5927.
(14) Shepard, S. G.; Fatur, S. M.; Rappé, A. K.; Damrauer, N. H. *J. Am. Chem. Soc.* **2016**, *138*, 2949.
(15) Ledwith, A. *Acc. Chem. Res.* **1972**, *5*, 133.
(16) Valentine, J. S. *Chem. Rev.* **1973**, *73*, 235.
(17) Wilke, G.; Schott, H.; Heimbach, P. *Angew. Chem., Int. Ed. Engl.* **1967**, *6*, 92.
(18) Holland, P. L. *Dalton Trans.* **2010**, *39*, 5415.
(19) Boisvert, L.; Goldberg, K. I. *Acc. Chem. Res.* **2012**, *45*, 899.
(20) Fogler, E.; Efremenko, I.; Gargir, M.; Leitus, G.; Diskin-Posner, Y.; Ben-David, Y.; Martin, J. M. L.; Milstein, D. *Inorg. Chem.* **2015**, *54*, 2253.
(21) Anson, C. W.; Ghosh, S.; Hammes-Schiffer, S.; Stahl, S. S. *J. Am. Chem. Soc.* **2016**, *138*, 4186.
(22) Douglas, J. J.; Cole, K. P.; Stephenson, C. R. J. *J. Org. Chem.* **2014**, *79*, 11631.
(23) Nicholls, T. P.; Constable, G. E.; Robertson, J. C.; Gardiner, M. G.; Bissember, A. C. *ACS Catal.* **2016**, *6*, 451.
(24) Pérez-Ruiz, R.; Domingo, L. R.; Jiménez, M. C.; Miranda, M. A. *Org. Lett.* **2011**, *13*, 5116.
(25) Yayla, H. G.; Peng, F.; Mangion, I. K.; McLaughlin, M.; Campeau, L.-C.; Davies, I. W.; DiRocco, D. A.; Knowles, R. R. *Chem. Sci.* **2016**, *7*, 2066.
(26) Johnson, M. W.; Hannoun, K. I.; Tan, Y.; Fu, G. C.; Peters, J. C. *Chem. Sci.* **2016**, DOI: 10.1039/C5SC04709A.
(27) Serpone, N.; Jamieson, M. A.; Henry, M. S.; Hoffman, M. Z.; Bolletta, F.; Maestri, M. *J. Am. Chem. Soc.* **1979**, *101*, 2907.
(28) Here the use of $[Cr]^{n+}$ indicates the charge for the entire complex. In places where the formal oxidation state of the metal ion is specified, we use Stock nomenclature.
(29) Li, Q.; Batchelor-McAuley, C.; Lawrence, N. S.; Hartshorne, R. S.; Compton, R. G. *J. Electroanal. Chem.* **2013**, *688*, 328.
(30) Pavlishchuk, V. V.; Addison, A. W. *Inorg. Chim. Acta* **2000**, *298*, 97.
(31) Demaille, C.; Bard, A. J. *Acta Chem. Scand.* **1999**, *53*, 842.
(32) McDaniel, A. M.; Tseng, H.-W.; Damrauer, N. H.; Shores, M. P. *Inorg. Chem.* **2010**, *49*, 7981.
(33) Shono, T.; Ikeda, A. *Chem. Lett.* **1976**, *5*, 311.
(34) Pfeil, A. *J. Am. Chem. Soc.* **1971**, *93*, 5395.
(35) Huber, K. P.; Herzberg, G. *Molecular Spectra and Molecular Structure IV. Constants of Diatomic Molecules*; van Nostrand Reinhold: New York, 1979.
(36) Wilkinson, F.; Brummer, J. G. *J. Phys. Chem. Ref. Data* **1981**, *10*, 809.
(37) Chen, C.-C.; Fox, M. A. *J. Comput. Chem.* **1983**, *4*, 488.
(38) Henriques, R. T.; Herdtweck, E.; Kühn, F. E.; Lopes, A. D.; Mink, J.; Romão, C. C. *J. Chem. Soc., Dalton Trans.* **1998**, 1293.
(39) Cismesia, M. A.; Yoon, T. P. *Chem. Sci.* **2015**, *6*, 5426.
(40) McQuilken, A. C.; Matsumura, H.; Dürr, M.; Confer, A. M.; Sheckelton, J. P.; Siegler, M. A.; McQueen, T. M.; Ivanović-Burmazović, I.; Moënne-Loccoz, P.; Goldberg, D. P. *J. Am. Chem. Soc.* **2016**, *138*, 3107.
(41) Krishnan, R.; Binkley, J. S.; Seeger, R.; Pople, J. A. *J. Chem. Phys.* **1980**, *72*, 650.
(42) Hay, P. J. *J. Chem. Phys.* **1977**, *66*, 4377.
(43) Austin, A.; Petersson, G. A.; Frisch, M. J.; Dobek, F. J.; Scalmani, G.; Throssell, K. *J. Chem. Theory Comput.* **2012**, *8*, 4989.
(44) Perdew, J. P.; Chevary, J. A.; Vosko, S. H.; Jackson, K. A.; Pederson, M. R.; Singh, D. J.; Fiolhais, C. *Phys. Rev. B: Condens. Matter Mater. Phys.* **1992**, *46*, 6671.
(45) Perdew, J. P.; Chevary, J. A.; Vosko, S. H.; Jackson, K. A.; Pederson, M. R.; Singh, D. J.; Fiolhais, C. *Phys. Rev. B: Condens. Matter Mater. Phys.* **1993**, *48*, 4978.
(46) Adamo, C.; Barone, V. *J. Chem. Phys.* **1999**, *110*, 6158.
(47) Perdew, J. P.; Burke, K.; Ernzerhof, M. *Phys. Rev. Lett.* **1996**, *77*, 3865.

(48) Perdew, J. P.; Burke, K.; Ernzerhof, M. *Phys. Rev. Lett.* **1997**, *78*, 1396.

(49) Scalmani, G.; Frisch, M. J.; Mennucci, B.; Tomasi, J.; Cammi, R.; Barone, V. *J. Chem. Phys.* **2006**, *124*, 094107.

(50) Martin, R. L. *J. Chem. Phys.* **2003**, *118*, 4775.

(51) Serpone, N.; Jamieson, M. A.; Hofmann, M. Z. *Inorg. Chim. Acta* **1978**, *31*, L447.

(52) Bauld, N. L. *Tetrahedron* **1989**, *45*, 5307.

(53) Slough, W. *Chem. Commun.* **1965**, 184.

(54) Krishna, M. C.; Grahame, D. A.; Samuni, A.; Mitchell, J. B.; Russo, A. *Proc. Natl. Acad. Sci. U. S. A.* **1992**, *89*, 5537.

(55) Samuni, A.; Krishna, C. M.; Mitchell, J. B.; Collins, C. R.; Russo, A. *Free Radical Res. Commun.* **1990**, *9*, 241.

(56) Reddan, J. R.; Sevilla, M. D.; Giblin, F. J.; Padgaonkar, V.; Dziedzic, D. C.; Leverenz, V.; Misra, I. C.; Peters, J. L. *Exp. Eye Res.* **1993**, *56*, 543.

(57) Song, L.; Trogler, W. C. *Angew. Chem., Int. Ed. Engl.* **1992**, *31*, 770.

(58) Connelly, N. G.; Geiger, W. E. *Chem. Rev.* **1996**, *96*, 877.

(59) Petronijević, F. R.; Nappi, M.; MacMillan, D. W. C. *J. Am. Chem. Soc.* **2013**, *135*, 18323.

(60) Griffin, J. D.; Zeller, M. A.; Nicewicz, D. A. *J. Am. Chem. Soc.* **2015**, *137*, 11340.

(61) Forster, L. S. *Chem. Rev.* **1990**, *90*, 331.

(62) Baltes, H.; Steckhan, E.; Schäfer, H. *J. Chem. Ber.* **1978**, *111*, 1294.

(63) Cerrai, P.; Guerra, G.; Tricoli, M.; Nucci, L. *Eur. Polym. J.* **1980**, *16*, 867.

(64) Nigenda, S. E.; Schleich, D. M.; Narang, S. C.; Kuemi, T. *J. Electrochem. Soc.* **1987**, *134*, 2465.

(65) Weber, J. M.; Rawls, M. T.; MacKenzie, V. J.; Limoges, B. R.; Elliott, C. M. *J. Am. Chem. Soc.* **2007**, *129*, 313.

(66) Beccia, M. R.; Biver, T.; García, B.; Leal, J. M.; Secco, F.; Venturini, M. *Inorg. Chem.* **2011**, *50*, 10152.

(67) We note that the chromyl species appears to reform divalent compound **1** when reducing agents are added to chromyl-containing solutions.

(68) Story, P. R.; Whited, E. A.; Alford, J. A. *J. Am. Chem. Soc.* **1972**, *94*, 2143.

(69) Lu, Z.; Parrish, J. D.; Yoon, T. P. *Tetrahedron* **2014**, *70*, 4270.

(70) Samoilova, R. I.; Crofts, A. R.; Dikanov, S. A. *J. Phys. Chem. A* **2011**, *115*, 11589.

(71) Initial concentrations of the dienophile and diene are 0.12 and 1.2 mM, respectively; the catalyst is present at 0.0012 mM concentration. Estimates of $O_2$ concentration in anhydrous $CH_3CN$ range from 1.26 mM (with 0.1 M $Bu_4NClO_4$)[31] to 2.42 mM in (salt-free).[64] Under saturated $O_2$ conditions, these concentrations jump to 6.3 and 12.1 mM, respectively.

(72) The literature quantum yield for $^1O_2$ production by $[(Cr(bpy)_3]^{3+}$ is 0.86, with a quenching rate constant of $2.5 \times 10^7$ $M^{-1} s^{-1}$.[65] Our *para*-anethole quenching rate constant is $9.5 \times 10^8$ $M^{-1} s^{-1}$.

(73) Crutchley, R. J.; Lever, A. B. P. *Inorg. Chem.* **1982**, *21*, 2276.

(74) Gonzales-Velasco, J.; Rubinstein, I.; Crutchley, R. J.; Lever, A. B. P.; Bard, A. J. *Inorg. Chem.* **1983**, *22*, 822.

(75) Hoffman, M. Z.; Bolletta, F.; Moggi, L.; Hug, G. L. *J. Phys. Chem. Ref. Data* **1989**, *18*, 219.

(76) Tiyabhorn, A.; Zahir, K. O. *Can. J. Chem.* **1996**, *74*, 336.

(77) Wrighton, M.; Markham, J. *J. Phys. Chem.* **1973**, *77*, 3042.

(78) Representative quenching rates for $[Ru(bpy)_3]^{2+}$ include 1,4-dinitrobenzene, $6.6 \times 10^9$ $M^{-1} s^{-1}$, and 4-methoxy-*N,N*-dimethylaniline, $5.0 \times 10^9$ $M^{-1} s^{-1}$; both in 0.1 M $Et_4NClO_4$ in $CH_3CN$.

(79) Parrish, J. D.; Ischay, M. A.; Lu, Z.; Guo, S.; Peters, N. R.; Yoon, T. P. *Org. Lett.* **2012**, *14*, 1640.